Journal of Materials Chemistry A

The Impact of Carbonation on Hydroxide Diffusion in Nano-Confined Anion Exchange Membranes

Journal:	*Journal of Materials Chemistry A*
Manuscript ID	TA-ART-01-2022-000830.R1
Article Type:	Paper
Date Submitted by the Author:	26-Mar-2022
Complete List of Authors:	Zelovich, Tamar; New York University, Chemistry Simari, Cataldo; University of Calabria Department of Chemistry and Chemical Technology, Department of Chemistry NICOTERA, Isabella; University of Calabria, Department of Chemistry and Chemical Tecnology Dekel, Dario; Technion Israel Institute of Technology, Chemical Engineering Tuckerman, Mark; New York University, Department of Chemistry and Courant Institute of Mathematical Sciences

The Impact of Carbonation on Hydroxide Diffusion in Nano-Confined Anion Exchange Membranes

Tamar Zelovich[(1)], Cataldo Simari[(2)], Isabella Nicotera[(2),(3)],

Dario R. Dekel[(4),(5)],and Mark E. Tuckerman[(1),(6),(7)*]

1) Department of Chemistry, New York University, New York, NY 10003, USA
2) Department of Chemistry and Chemical Technologies, University of Calabria, Via P Bucci, 87036 Rende CS, Italy
3) CNR-ITAE "Nicola Giordano", Via Salita S. Lucia sopra Contesse 5, Messina, 98126, Italy
4) Wolfson Department of Chemical Engineering, Technion – Israel Institute of Technology, Haifa, 3200003, Israel
5) Nancy & Stephen Grand Technion Energy Program, Technion – Israel Institute of Technology, Haifa, 3200003, Israel
6) Courant Institute of Mathematical Sciences, New York University, New York, NY 10012, USA
7) NYU-ECNU Center for Computational Chemistry, NYU Shanghai, 3663 Zhongshan Rd N, Shanghai 200062, China

Email: mark.tuckerman@nyu.edu

Abstract

Exposing anion exchange membrane (AEM) fuel cells to ambient air is known to decrease fuel cell efficiency significantly due to the presence of CO_2. In this combined theoretical and experimental study, we examine the hydration conditions that promote reactions between CO_2 and hydroxide ions in nano-confined AEMs, and we explore the effect of the carbonation process on the solvation structure and diffusion of hydroxide ions. Using fully atomistic *ab initio* molecular dynamics (AIMD) simulations, we find that increasing hydration can delay the carbonation reaction between OH^- and CO_2. Once reacted, HCO_3^- ions exist along the simulation, which significantly reduce the diffusion of the hydroxide ions. We confirm these results using ^{1}H- and ^{13}C-pulsed field gradient nuclear magnetic resonance. AIMD simulations further reveal that the HCO_3^- actively "blocks" the diffusion path of hydroxide ions along the simulation cell. We expect that elucidating the key design principles underlying the atomistic effects of carbonate ions on hydroxide ions diffusion mechanisms in model AEMs will provide useful guidelines for the synthesis and experimental characterization of novel highly conductive AEMs fuel cell technologies in the presence of CO_2 containing air.

TOC:

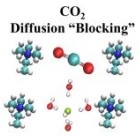

1. Introduction

In recent years, anion-exchange membrane fuel cells (AEMFCs) have received significant attention, as this technology allows for the removal of expensive Pt catalysts from their structure, ultimately promising affordable fuel cells for massive energy conversion applications.[1-12] However, one significant challenge that currently prevents this technology from successful commercialization is the chemical stability of the polymer electrolyte. It has been shown that cation instability in anion-exchange membranes (AEMs) stems mainly from the chemical degradation of the cationic functional groups.[13-15] A second major challenge, which has received less attention thus far, concerns the carbonation process that occurs when AEMFCs operate with ambient (CO_2 containing) air.[16] It has recently been shown that when the system is exposed to ambient air, the hydroxide ion conductivity in AEMs decreases significantly because of the carbonation reactions between OH^- and CO_2: [17-23]

$$OH^- + CO_2 \leftrightarrows HCO_3^- \quad (1)$$

$$OH^- + HCO_3^- \leftrightarrows CO_3^{2-} + H_2O \quad (2)$$

As the carbonation reaction reduces the hydroxide ion conductivity over time, this process is expected to cause significant reductions in the AEMFC performance and efficiency. Most theoretical and experimental studies in this area focus on identifying the conditions required to prevent the carbonate reaction and to reduce the amount of the three carbon-containing species CO_2, HCO_3^- and CO_3^{2-} in the membrane. Nevertheless, very little is known about the effect of these molecules on the solvation structures and interactions of the hydroxide ions with the functional groups. Such effects are expected to be more pronounced in low-hydration conditions, as there are insufficient water molecules to fully solvate the hydroxide ions.[22,24,25] Studying the effect of the three carbon-containing species on the hydroxide ion solvation shells will provide critical information on the reactivity and diffusivity of the

hydroxide ions in a mixed environment of hydroxide and carbonate ions, which simulates real ambient air-fed AEMFC environments.

The experimental investigations of CO_2 in AEMs include the effect of the three carbon-containing species (i.e., CO_2, HCO_3^- and CO_3^{2-}) on the hydroxide ion diffusion. At present, most of the theoretical studies in this field are forced to study the effect of only one of the three carbon-containing species on the hydroxide solvation structure and diffusion[22], as they are based on fixed-charge empirical force fields, which are not reactive and cannot describe many-body polarization effects. This approximation makes it difficult for molecular dynamics (MD) simulations to describe chemical bond-breaking and forming events, which are crucial for exploring chemical reactivity. Hence, empirical force-field studies force the system to stay at a specific equilibrium, which does not necessarily represent realistic conditions the system might be expected to reach. To the best of our knowledge, a deeper atomistic understanding as part of the dynamic process is still missing. *Ab initio* Molecular Dynamics (AIMD) methods [26,27] offer the ability to explore ion dynamics driven by electronic structure calculations performed "on the fly," thereby overcoming the difficulties of MD simulations.

Recently, nano-confined environments have been used to investigate cost-effective and reliable polymer architectures for use in electrochemical devices.[28-38] In our previous studies, we employed tailored nano-confined structures to mimic certain features of ion-conducting polymer membranes with the aim of uncovering key influences on hydroxide diffusivity in AEMs.[39-45] These investigations showed that water molecules exhibit unusual structures that depend on the system size and water density. The hydroxide diffusion mechanism, which has been widely studied and well-characterized in bulk aqueous basic solution[46-61], was strongly dependent on the intriguing water structure under confinement. [39-45]

In this work, we report a combined theoretical and experimental investigation of the effect of the carbonation process on the diffusivity of hydroxide ions and water molecules in architecturally distinct AEMs with trimethyl-alkyl ammonium ions (TMA) at different hydration levels. Additionally, we explore the conditions that promote reactions (1) and (2) in nano-confined environments, under low-hydration conditions. The theoretical component, performed in a nano-confined region between two graphane sheets to which TMA ionic functional groups are attached with a simple linker, employed fully atomistic AIMD

simulations.[26,27] In an attempt to capture the experimental picture and to fully explore the effect of the three carbon-containing species on the hydroxide ion diffusion, we designed six different model AEMs; five systems represent the initial condition of the forward path of reaction (1), and the sixth system represents the initial conditions of the backward path of reaction (2). For each model, we analyze the water structure and the hydroxide ion diffusion using the protocol described in our previous studies. [39-45]

The experimental study includes a measurement of the diffusivity of the water/hydroxide and carbon species in polysulfone (PSU)-TMA-based AEMs, at two different hydration conditions, using ^{1}H- and ^{13}C-Pulsed Field Gradient (PFG) Nuclear Magnetic Resonance (NMR).[62-64] Results are qualitatively compared to those obtained by AIMD simulations.

2. Description of Systems

Previous coarse-grained studies of TMA-tethered triblock copolymers suggested a lamellar morphology for this type of membrane.[65] Following our previous work [39-45], we designed six idealized models of AEM environments. As a mimic of the PSU backbone used in this study, our theoretical model employs a graphane bilayer (GB) with a variable number of TMA cations tethered inside by short carbon chains. [66–70] The remaining free volume between the graphane layers is filled with water to a desired hydration level (defined as λ, the number of water molecules per cation) and a variable number of hydroxide ions (with oxygen atoms denoted as O^*_1 and O^*_2). The cations are attached to fixed points on one side of the GB but are otherwise free to move in the aqueous environment. Figure 1 shows the distance between the attachment points, which defines the polymer electrolyte cation spacing in the *x* and *y* directions. As a result, the simulation cell is partitioned into an open region, which we refer to as center of the cell region (CCR), and constricted regions between the cations, which we refer to as bottleneck regions (BR). [40,42-44]

The five representative systems (**C1**, **C2**, **C3**, **C4**, **C10**; C indicating the presence of CO_2 in the initial structures and the number representing the hydration value λ) contain two TMA cations, two hydroxide ions, and one CO_2; the sixth system (**3T3C**; 3T indicating the number of cations, 3 representing the hydration value, and C denoting the presence of one CO_3^{2-} in the

initial structure) contains three TMA cations, one hydroxide ion, and one CO_3^{2-} ion. The tunable parameters used to generate the systems are: (i) the hydration level, chosen to be 1, 2, 3, 4 and 10 (see SI for further explanation regarding the choice of λ); (ii) the distance between the two carbon sheets, Δ*z*, chosen to achieve the highest water density possible (see Refs. [39-45] and Supporting Information (SI) for rationale); and (iii) the polymer electrolyte cation spacing in the *x* and *y* directions (Δ*x* and Δ*y*), in which Δ*x* is fixed at 10 Å and Δ*y* is fixed at 6.6 Å, for all systems. The six architecturally distinct cells in this study were designed to obtain significantly different water distributions. Systems **C2, C3**, **C4**, and **C10** will be compared to similar, previously studied systems without the presence of CO_2 in the initial structures (see Refs. [39,40]).

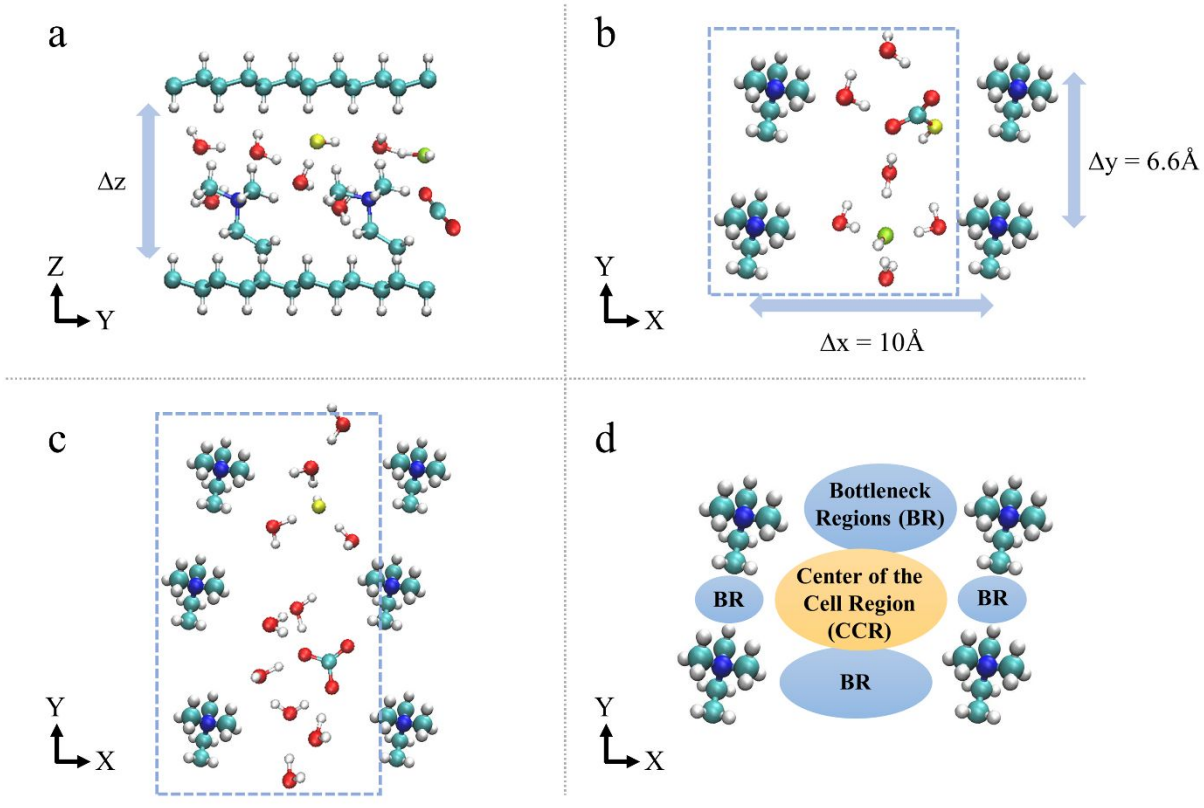

Figure 1: (a) A side perspective of the atomistic graphane bilayer (GB) systems each consisting of two graphane sheets, two TMA cations, two hydroxide ions, one CO_2, and enough water molecules to reach the required value of λ, representing the initial structure of systems **C1**, **C2**, **C3**, **C4**, and **C10**. (b) The view of a typical cell from a *z*-perspective for systems **C1**, **C2**, **C3**, **C4**, and **C10,** after reaction (1) occurred, consisting of one hydroxide ion and one HCO_3^-. (c) The initial structure of model **3T3C** from a *z*-perspective, consisting of three TMA cations, one hydroxide ion, and one CO_3^{2-}. (d) The view of a cell

from a *z*-perspective, containing only TMA cations. The blue and orange areas indicate the bottleneck regions (BR) and the center of the cell region (CCR), respectively. The graphane bilayer atoms (C and H atoms) were removed from figures (b), (c) and (d) to better show the cation structures. The GB systems are fully hydrogenated except for the attachment points of the cations. The blue rectangles show the primitive simulation cell of the system. The turquoise arrows demonstrate the polymer electrolyte cation spacing along the *x, y,* and *z* directions (Δx, Δy, and Δz). The red, white, turquoise, and blue spheres represent O, H, C, and N atoms, respectively. Yellow and green spheres represent the hydroxide and HCO_3^- ions.

3. Method Section

3.1. Computational Method

After obtaining the desired starting structures, AIMD simulations [26,27] were run using the CPMD code. [27,71] Each system was equilibrated at room temperature using a massive Nosé-Hoover chain thermostat [72], followed by 15-20 ps of canonical (NVT) dynamics, also using a Nosé-Hoover chain thermostat, and finally ~80 ps of microcanonical (NVE) dynamics. Dispersion forces were included via the Dispersion-Corrected Atomic Core Pseudopotentials (DCACP) scheme within the Kohn-Sham formulation of Density Functional Theory and the B-LYP exchange-correlation functional. [73,74] The performance B-LYP+DCACP has previously been shown to provide satisfactory results for water-acene interactions [75] and for liquid water. [76] All radial distribution functions (RDFs) and coordination numbers (CNs) were calculated using both the NVT and NVE trajectories, while all dynamical properties were obtained using only the NVE trajectories. A detailed description of the computational method can be found in the SI and in our previous work. [39-45]

3.2. Experimental Method

PSU-TMA AEMs were synthesized based on the same chemistry (Figure 2). The AEMs were converted into their hydroxide, HCO_3^-, and mixed forms by exchanging their counter-ions to OH^-, HCO_3^-, and mixed OH^-/ HCO_3^-, respectively (Figure S6). The synthesis and procedure are briefly discussed in the SI. ^{1}H- PFG NMR [44] was used to measure the diffusivity of water and ionic species through the AEMs in their three ionic forms. To study the effect of hydration, the diffusivity measurements were carried out on the AEMs at two different hydration levels (λ

= 4, 10). The ^{1}H-NMR signal is large and comprises all the ^{1}H-nuclei present in the system; therefore, the diffusivity measurement reflects the behavior of all H-containing species, e.g., H_2O, OH^- and HCO_3^-. To distinguish between the diffusivity of hydroxide and HCO_3^- anions, for the case of AEM in its mixed OH^-/ HCO_3^- form, ^{13}C- PFG NMR was used to measure the diffusivity of the C-containing species, e.g., HCO_3^-, making a comparison between experimental and theoretical results possible. Full details concerning membrane synthesis and NMR experiments are described in the SI and in Refs. [44,77].

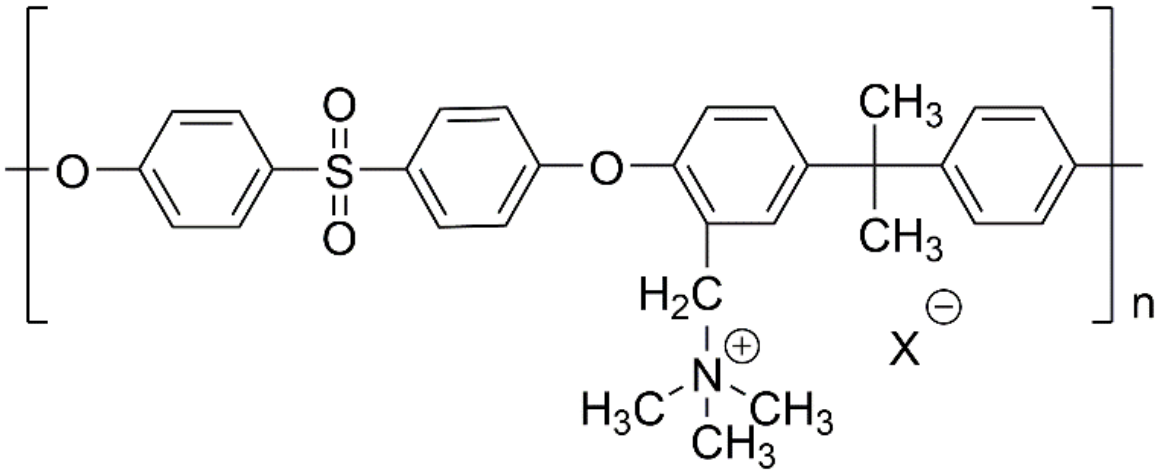

Figure 2: Chemical structure of the PSU-TMA AEM used for the NMR diffusivity measurements. AEM samples were converted into their OH^-, HCO_3^-, and mixed forms by converting the counter-ions (X^-) into OH^-, HCO_3^-, and mixed OH^-/ HCO_3^-, respectively.

4. Results

4.1 Effect of Hydration on Reactions (1) and (2)

Previous studies have shown that the reaction barrier along the forward path of reaction (1), i.e., $OH^- + CO_2 \rightarrow HCO_3^-$, in bulk aqueous solution involves bringing OH^- into the first solvation shell of CO_2, followed by bending of CO_2. [78-82] This is achieved by decreasing the number of water molecules solvating the hydroxide ions from 4 to 2.5, thus additionally decreasing the coordination number (CN) of the CO_2, which leads to a distortion of the O-C-O angle. For the reverse reaction, i.e., $HCO_3^- \rightarrow OH^- + CO_2$, the activation free energy is significantly larger than that of the forward reaction, as the dominant part of the activation

energy must break the strong C-O bond. For reaction (2), (i.e., $OH^- + HCO_3^- \leftrightarrows CO_3^{2-} + H_2O$), previous studies have shown that the backward path is preferable when CO_3^{2-} does not reach complete solvation. [83-86] This suggests that the reaction barrier for the forward path of reaction (1) and the backward path of reaction (2) will be reduced under low-hydration conditions, which results in the creation of HCO_3^-.

In order to shed light on the energy barrier of these two reactions in nano-confined environments under low-hydration conditions, we follow the number of hydroxide ions in each model AEM along the AIMD trajectory (see Figure 3). For systems **C1**, **C2**, **C3**, **C4**, and **C10**, two hydroxide ions correspond to the presence of CO_2 (i.e., the initial structure), one hydroxide ion corresponds to the presence of HCO_3^- (i.e., the forward path of reaction (1) occurred), and zero hydroxide ions correspond to the presence of CO_3^{2-} (i.e., both the forward path of reactions (1) and (2) occurred). For system **3T3C**, one hydroxide ion corresponds to the presence of CO_3^{2-} (i.e., the initial structure), while two hydroxide ions correspond to the presence of HCO_3^- (i.e., the backward path of reaction (2) occurred). For the least hydrated system **C1**, we find that both the forward path of reactions (1) and (2) occurred, and that reaction (2) is in equilibrium for most of the simulation time (see Figure 3). As hydration increases (i.e., systems **C2**, **C3**, **C4**), the preferable state of the system includes one hydroxide ion and one HCO_3^- (i.e., the forward path of reaction (1) occurred). For the most hydrated system, **C10**, the forward path of reaction (1) did not occur as there are two hydroxide ions along the entire simulations. For system **3T3C** (with only one hydroxide ion in the initial state) the number of hydroxide ions increases to two for ~80% of the simulation time (i.e., the backward path of reaction (2) occurred) and reaction (2) is in equilibrium for most of the simulation time.

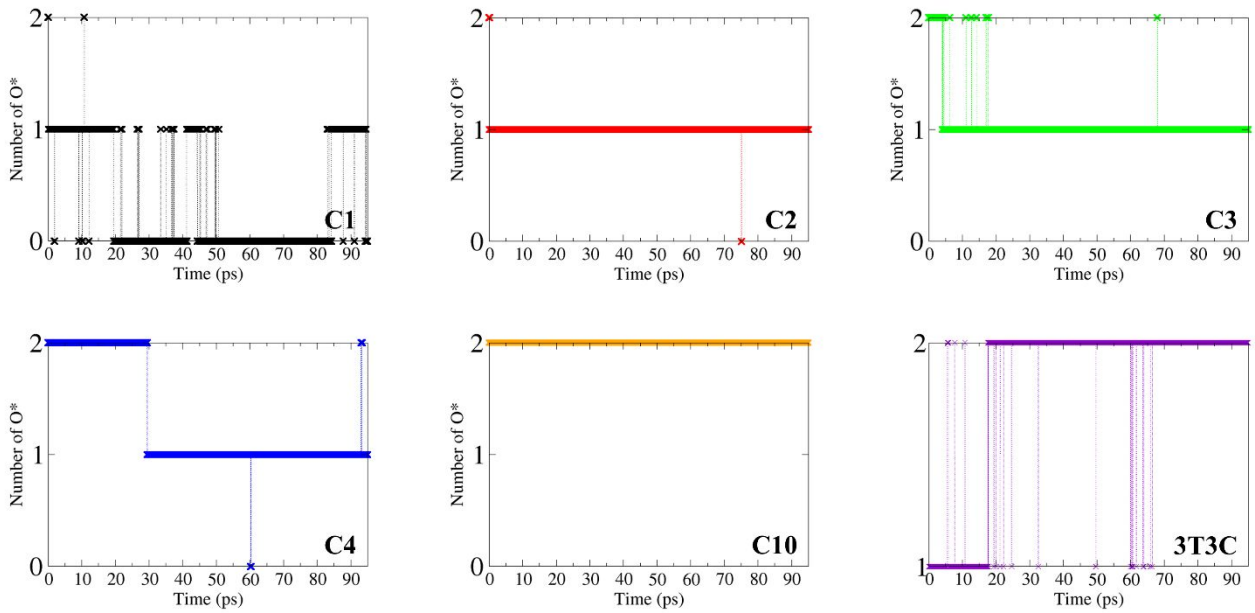

Figure 3: Number of hydroxide ions as a function of time for systems **C1**, **C2**, **C3**, **C4**, **C10**, and **3T3C**.

In order to estimate the effect of hydration on the kinetics of reaction (1), Figure 4 presents the time required for the forward path of the 1st reaction to occur ($OH^- + CO_2 \rightarrow HCO_3^-$) for systems **C1**, **C2**, **C3**, and **C4**, as a function of λ, which shows that the reaction is delayed by an increase in hydration (the inset presents the time it took for the 1st and 2nd reactions to occur for all systems).

Figures 3 and 4 show that, for low to moderate hydration values ($\lambda < 10$), exposing nano-confined AEMs to ambient air results in production of HCO_3^- in the system. However, keeping the system hydrated ($\lambda \geq 10$) can delay the carbonation reactions between OH^- and CO_2, hence delaying the effect of the carbonation process on AEM performance.

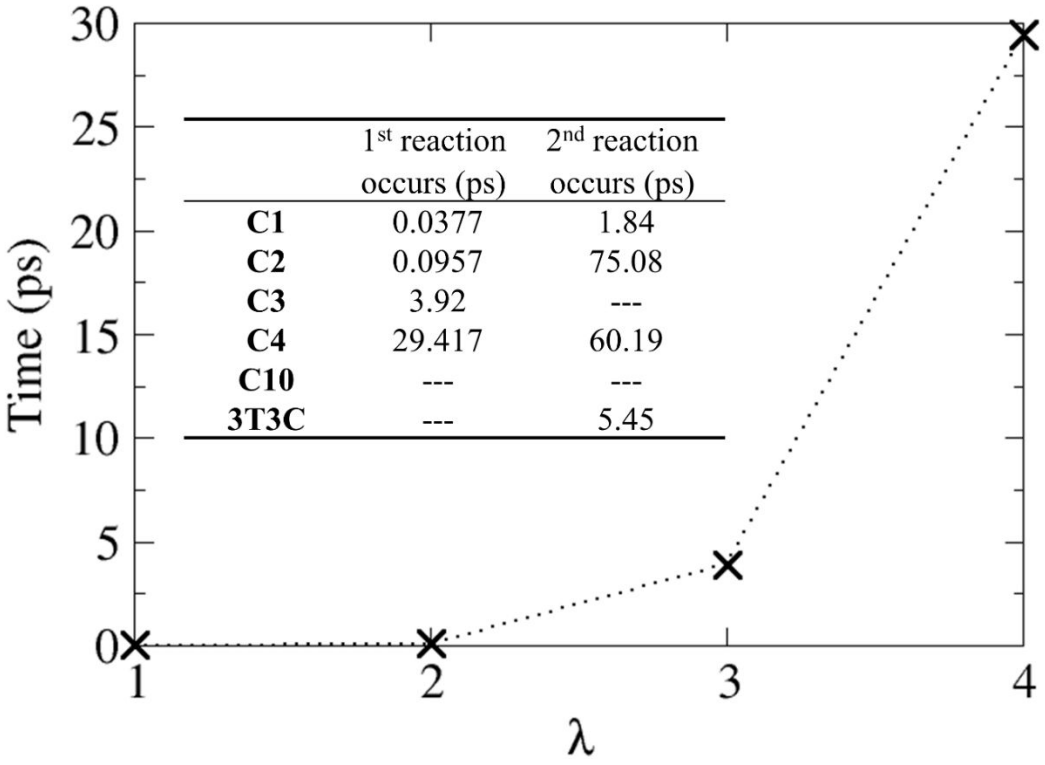

	1st reaction occurs (ps)	2nd reaction occurs (ps)
C1	0.0377	1.84
C2	0.0957	75.08
C3	3.92	---
C4	29.417	60.19
C10	---	---
3T3C	---	5.45

Figure 4: The time (in ps) required for the forward path of the 1st reaction to occur ($OH^- + CO_2 \rightarrow HCO_3^-$) for systems **C1**, **C2**, **C3**, and **C4**, as a function of λ. Inset: The time (in ps) required for the 1st and 2nd reactions to occur for all systems. To ensure the above results, we present in the SI Table S4 similar results at different initial conditions.

Figure 5 shows snapshots from the trajectory of system **C4** and describes the steps of the reaction $OH^- + CO_2 \rightarrow HCO_3^-$ in the nano-confined model AEM environment. First, the hydroxide is solvated with four water molecules (Figure 5a). Next, the CN of the hydroxide ion is reduced to three, in which there are no water molecules between the hydroxide ion and CO_2 (Figure 5b), which allows the hydroxide ion to penetrate into the first solvation shell of CO_2, followed by a bend in the O-C-O angle (Figure 5c). Finally, a bond is formed between OH^- and CO_2 to create HCO_3^- (Figure 5d). Combining the results from Figures 3 through 5, we conclude that, when compared to bulk solution, the hydroxide is more likely to penetrate into the first solvation shell of CO_2 at low-λ AEMs, which results in the following reaction: $OH^- + CO_2 \rightarrow HCO_3^-$. These results validate the hypothesis that the reaction barrier for the forward path of reaction (1) will be reduced under low-hydration conditions.

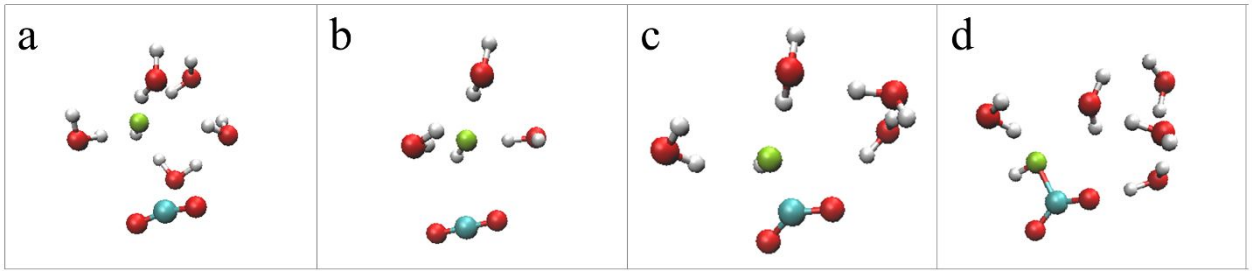

Figure 5: Representative configurations showing the proposed reaction path of $OH^- + CO_2 \rightarrow HCO_3^-$ for low hydrated model AEM, including important water molecules from the first and second solvation shells of the hydroxide ion (figures taken from the trajectory of system **C4**). See main text for further explanation.

4.2 Solvation Structures

4.2.1 Water Structure

In previous studies of AEM at low hydration levels ($\sim\lambda < 8$), we found that the water distribution in AEM is not-uniform. [40,43] All water molecules in these systems can be regarded as interfacial, i.e., in contact with some part of the "membrane" and are inhomogeneously distributed throughout the system. Unlike in bulk solution, in which the water oxygen has an average of a fourfold-tetrahedral coordination pattern [46,47], the non-uniform water distribution results in a first solvation shell of either zero, one, or two for the water oxygens. Additionally, the non-uniform water distribution refers to the formation of spatially separated (by ~4 Å) water clusters in the vicinity of each ion. As a result, void areas are formed in the simulation cell. The specific patterns formed in these clusters influence the solvation structure and diffusion mechanisms of the hydroxide and carbonate ions as will be discussed next. The OO and NO_w RDFs and CN values for the six systems are shown in the SI, to demonstrate the water oxygens solvation shells.

4.2.2 CO_2 / HCO_3^- / CO_3^{2-} Structure

In order to gain a better understanding of the solvation structures of the carbon-containing species, we show, in Figures 6a and 6b, the CO RDFs and CNs, in which C represents the carbon atoms of either CO_2, HCO_3^- and CO_3^{2-}, and O represents all oxygens in the system. The first solvation shell peak is located at 1.3 Å for all systems, in which the shoulder

seen for systems **C1**, **C2**, **C3**, and **C4** at 1.4 Å represents the transition between CO_2 to HCO_3^-. The CN of the first solvation shell reflects the most common carbonate species found along the simulation for each of the systems. Hence, in agreement with the results presented in Figure 3, we find that the CN for systems **C1**, **C2**, and **C3** is 3, thus corresponding to the appearance of HCO_3^- for nearly the entire simulation; for system **C4** the CN is 2.8, which corresponds to the appearance of HCO_3^- for ~70% of the simulation time; for system **C10** it is 2, which corresponds to the appearance of CO_2 for the entire simulation; for system **3T3C,** the CN is 3, which corresponds to the appearance of HCO_3^- and CO_3^{2-} for the entire simulation. The CN of the second solvation shell is 5.7, 6.0, 6.1, 6.5, 7.4, and 11.2 for systems **C1**, **C2**, **C3**, **3T3C**, **C4**, and **C10**, respectively. For systems **C2**, **C3**, **C4**, and **3T3C**, in which the carbon atom represents HCO_3^-, the CN value for the second solvation shell is considered low when compared to bulk solution, where it was found to be 9.9. [78-82] Inspecting the configurations from the NVE trajectory reveals that HCO_3^-, which is considered to be a larger anion than OH^-, occupies a much larger space than the hydroxide ion in the simulation cell. Due to this geometric restriction, the TMA cations interrupt the water molecules from penetrating into the HCO_3^- first and second solvation shells, which explains the low CN values found for HCO_3^- (e.g., see inset of Figures 6a and 6b).

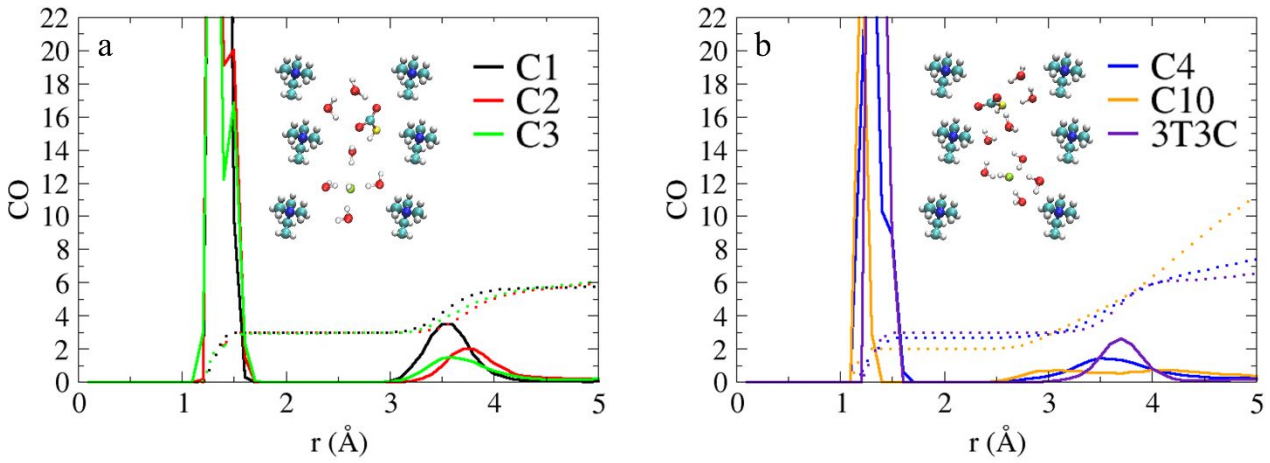

Figure 6: CO RDFs of systems (a) **C1**, **C2**, **C3** and (b) **C4**, **C10**, and **3T3C** (represented by black, red, green, blue, orange and purple curves, respectively). Colored dotted lines show the coordination numbers (CNs) for each system. Inset: an example for the HCO_3^- structure taken from the trajectory of (a) system **C3** and (b) system **C4**.

4.2.3 OH^- Structure

Figure 7A presents the O*O RDFs and CNs of systems **C2**, **C3**, **C4**, **C10**, and **3T3C** (system **C1** is not presented as there are no hydroxide ions in the system for most of the simulation). For systems **C2**, **C3**, **C4**, and **C10**, we compare the results for previous systems studied without the presence of CO_2 in the initial structure (taken from Refs. [39,40,44]). For all systems, with and without the presence of the carbon-containing species, the first solvation shell of the hydroxide oxygen is located at 2.7 Å, as reported for bulk solution. [46-55] The effect of the three carbon-containing species on the hydroxide solvation structure is noticeably pronounced in the CN of the first and second solvation shells (see Figure 7B), as we find that adding CO_2 to the initial structure increases the number of water oxygens surrounding the hydroxide ions for systems **C2**, **C3**, **C4**. For system **3T3C**, we find a high CN value as found for systems **C3** and **C4**. However, for system **C10**, which does not count as a low-hydrated system, we find that adding CO_2 to the system did not change the hydroxide ions solvation shells (see SI for exact CN values).

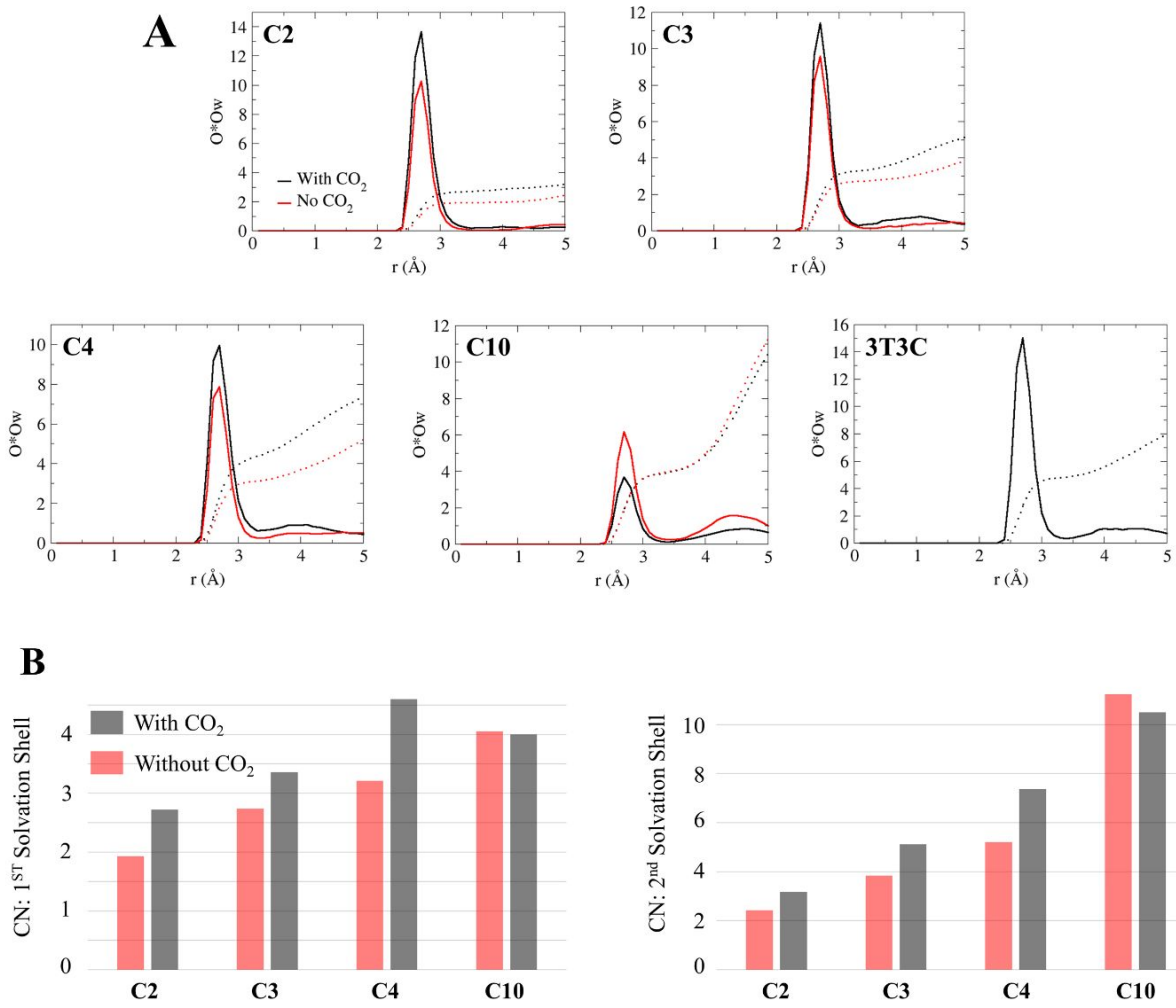

Figure 7: (A) O^*O_w RDFs of systems **C2**, **C3**, **C4**, **C10**, and **3T3C**, with and without CO_2 in the initial structure (black and red curves, respectively). Colored dotted lines show the CNs for each system. (B) Summarized CNs of water molecules in the first and second solvation shells around hydroxide ions for systems **C2**, **C3**, **C4**, and **C10**, with and without CO_2 in the initial structure. Data for systems without carbon-containing species were taken from Refs. [39,40,44].

In order to shed additional light on the high hydration around the hydroxide ions, we turn back to Figures 3 and 6 and to the NVE trajectory. As discussed in Figure 3, systems **C2**, **C3**, and **C4**, has one OH^- and one HCO_3^- in the system, unlike two hydroxide ions for systems without carbon-containing species in Refs. [39,40,44]. As shown in Figure 6, as a result of the large size of HCO_3^- and the geometric constrictions of the TMA cations, the solvation shell of HCO_3^- is restricted. Hence, the water molecules in the systems are divided between one OH^- and

one HCO_3^-, in which HCO_3^- cannot achieve a full solvation shell. As a result, the water molecules are drawn towards the hydroxide ion and less towards HCO_3^-.

The effect of the high hydration around the hydroxide ions is seen in the NO* RDFs and CNs shown in Figure 8, where we compare the results for previous systems studied without the presence of the three carbon-containing species (taken from Refs. [39,40,44]). For systems **C2** and **C3**, we find that the hydroxide ions are located further from the cations in the presence of carbonate anion. Additionally, for systems **C2, C3** and **C4**, we find a decrease in the CN of the first solvation shell, in the presence of carbonate anion. These results suggest there is an increase in the shielding between the hydroxide ions and the TMA functional group, pushing the hydroxide further away from the TMA cations, which, in turn, can decrease the degradation process, as was recently reported in Ref. [22].

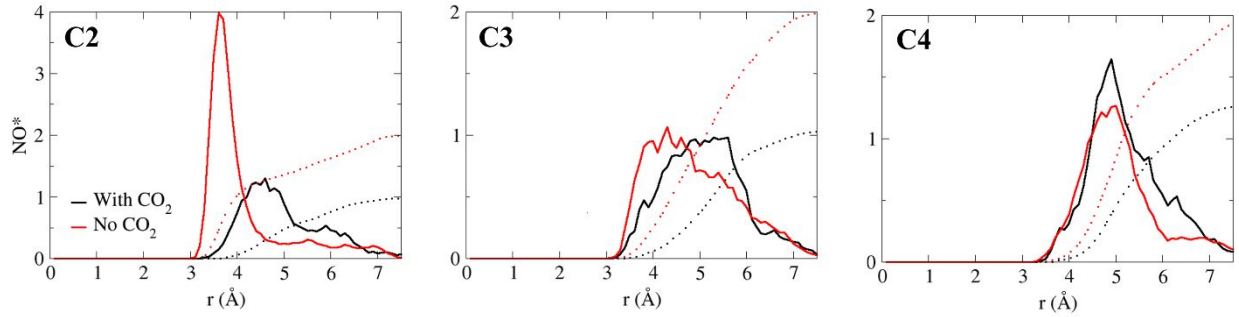

Figure 8: NO^* RDFs of systems **C2**, **C3**, and **C4**, with and without CO_2 in the initial structure (black and red curves, respectively). Colored dotted lines show the CNs for each system. Data for systems without CO_2 in the initial structure were taken from Refs. [39,40,44]. See SI for NO^* RDFs CNs for all systems, and for a more detailed description on the RDFs and CNs results.

4.3 Dynamical Results

Next, we explore the effect of CO_2 , HCO_3^- , and CO_3^{2-} on hydroxide ion diffusion. The picture of the dynamics emerges from a calculation of the average diffusion coefficient of the hydroxide ions, water molecules, and the three carbon-containing species in each of the model AEMs. Table 1 compares the diffusion constants of the hydroxide ions and water molecules to systems without the presence of CO_2 in the initial structure, as found in Refs. [39,40,44].

Table 1: Diffusion constants obtained from the slope of the mean square displacement in units of 10^{-4} cm^2/s (i.e., $Å^2/ps$). *Results taken from Refs. [39,40,44]. See SI for diffusion coefficients along each of the axes separately.

		D_{OH^-}	D_{H_2O}	$D_{CO_2\,/\,CO_3^{2-}\,/\,HCO_3^-}$
C1	W CO_2	0.00	0.10	0.00
C2	W CO_2	0.04	0.02	0.00
	*WO CO_2	0.01	0.04	0.00
C3	W CO_2	0.03	0.05	0.00
	*WO CO_2	0.15	0.09	0.00
C4	W CO_2	0.06	0.07	0.02
	*WO CO_2	0.17	0.06	0.00
C10	W CO_2	0.06	0.04	0.00
	*WO CO_2	0.12	0.01	0.00
T3C3	W CO_3^{2-}	0.02	0.03	0.00

As stated above, we find that the hydroxide ions are more hydrated in systems **C2**, **C3**, **C4**, and **3T3C**, which suggests that these systems have the potential to increase their conductivity. However, for systems **C2**, **C3**, **C4**, and **C10**, where there is a comparison with systems without the presence of carbon-containing species, we find that the hydroxide ions diffusion is reduced more than twofold for systems **C3**, **C4**, and **C10**, and remains non-diffusive with a diffusion coefficient lower than 0.1 $Å^2/ps$ for system **C2** (see Refs. [39,40,44] for a detailed definition of a non-diffusive hydroxide ion). Additionally, we find that the water diffusivity remains low for all systems. As expected, we find that the three carbon-containing species are non-diffusive for all systems, as these species are considered to be larger and less mobile than the hydroxide ions. [87] To demonstrate the low diffusion of both the hydroxide and carbonate ions in these systems in greater detail, we plot the coordinates of the hydroxide oxygen atoms and the carbonate atoms as a function of time in the SI.

The non-diffusivity of the carbonate ions, and the low diffusivity of the hydroxide ions in the presence of carbonate ions, have been confirmed by experimental NMR measurements in PSU-TMA-based AEMs for systems under λ = 4 and 10 (details concerning membrane synthesis and NMR experiments are described in the SI). Diffusivity values measured in the synthesized AEMs in their hydroxide and HCO_3^- form (Figure 9) show that, in both λ = 4,10 levels, the total diffusivity of all species, measured by ^{1}H NMR, are significantly higher in the AEMs where the hydroxides are the only ionic species present (OH^- form), as compared to the AEMs in which the carbonate are the only ions present (HCO_3^- form). For instance, the diffusivity measured in OH^- form and HCO_3^- form were 2 to 5 times higher and 3 to 10 times higher, at λ = 4 and λ = 10, respectively. Interestingly, at high hydration levels of λ = 10, the effect of the carbonate ions onto the diffusivity in the AEM is significantly more pronounced. This is consistent with experimental results recently reported, where the effect of the CO_2 onto the overall performance in the AEMFC was significantly more pronounced (higher CO_2-related overpotential losses) with AEMs with higher hydroxide conductivity (higher hydration levels).[23] In addition, diffusivity measurements of AEMs in their mixed OH^-/HCO_3^- were also added for comparison (Figure 9). As expected, the diffusivity values of the species in the AEM in their mixed ionic form falls in between those of 'pure' hydroxide and carbonate forms, confirming the effect of the carbonate ions onto the diffusivity of the species, as found in the AIMD simulations described above. For the mixed ionic form of the membrane, we also measured the diffusion of the ^{13}C (Figure 9c). In this way we differentiate the diffusivity of the carbonate from the diffusivity of the hydroxide and water. As was predicted by our AIMD simulations, the diffusivity of the carbonate was lower than that measured for the hydroxide and water (^{1}H). Interestingly, the difference between the diffusivity of carbonate and that of the hydroxide/water is larger at lower temperatures.

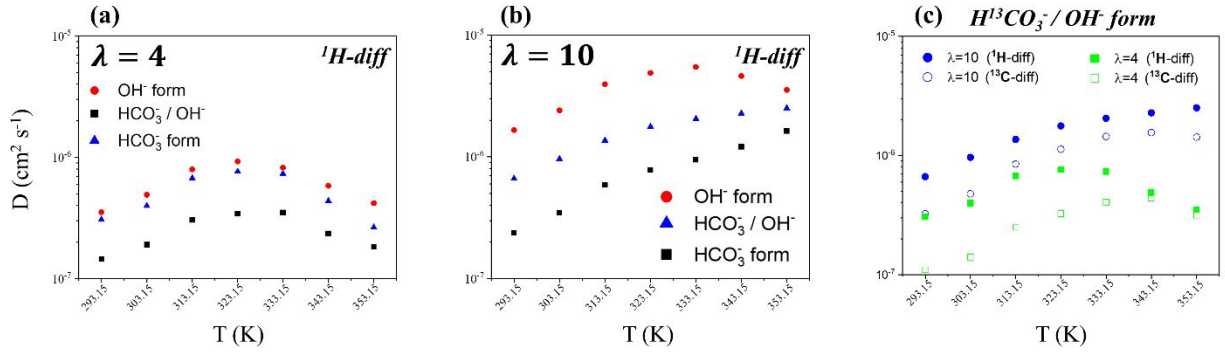

Figure 9: Self-diffusion coefficients of hydroxide ions and HCO_3^-confined in water swelled AEMs in their OH^-, HCO_3^-, and OH^-/HCO_3^- mixed forms, measured at hydration levels of (a) $\lambda = 4$, (b) $\lambda = 10$, and (c) $\lambda = 4$ and 10, in their $OH^-/H^{13}CO_3^-$ mixed forms measured on both ^{13}C and ^1H.

Inspection of the configurations from the AIMD trajectories reveals that the low diffusivity of the hydroxide ions in the presence of carbonate ions in model AEMs derives from the non-diffusivity of the carbonate ions, as it is actively "blocking" the hydroxide ions from diffusing along the simulation cell and in particular to diffuse along the BR. Figure 10 demonstrates the HCO_3^- "blocking" mechanism of the hydroxide diffusion at these low hydrated conditions. As shown, the hydroxide ions are located at the BR in a stable threefold structure (Figure 10a). [39,40] Once the first solvation shell of the hydroxide is reduced to one, and it is located in the first solvation shell of HCO_3^-, a hydrogen bond (HB) is formed between the hydroxide ion and HCO_3^- (Figure 10b). Next, a proton transfer (PT) event occurs between the hydroxide ion and HCO_3^-, according to the reaction: $OH^- + HCO_3^- \rightarrow CO_3^{2-} + H_2O$ (Figure 10c). As a result, there are no hydroxide ions in the system. After a few picoseconds, a HB is formed between CO_3^{2-} and a nearby water molecule (Figure 10d). Next, a PT occurs between CO_3^{2-} and a water molecule, creating HCO_3^- and a hydroxide ion, according to the backward path of reaction (2): $CO_3^{2-} + H_2O \rightarrow OH^- + HCO_3^-$ (Figure 10e). The hydroxide ion continues to diffuse back into the CCR, where it was originally located (Figure 10f). Figures 10g and 10h present an ideal water structure in the BR with and without a hydroxide ion.

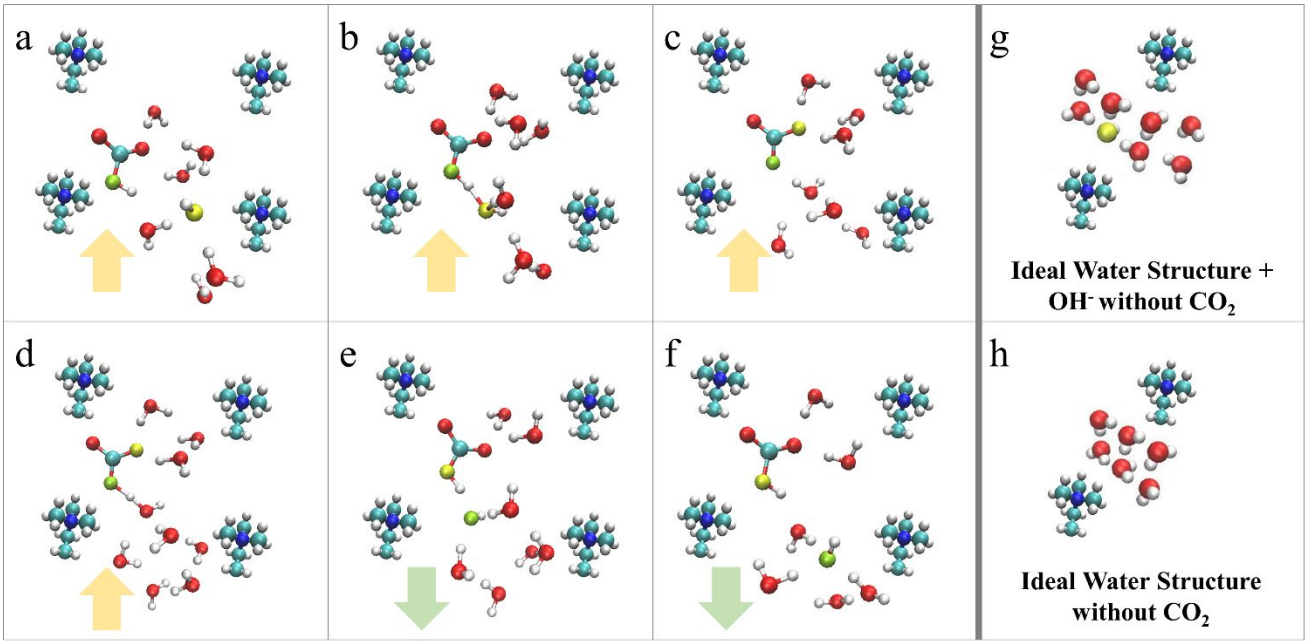

Figure 10: Representative configurations showing the proposed "HCO_3^- blocking" of the hydroxide ion diffusion, taken from the trajectory of system **C4**, including important water molecules from the first and second solvation shells of the hydroxide ion. (a) The hydroxide ion is entering the BR in a stable threefold structure. (b) The hydroxide ion is located in the BR with only one water molecule in the first solvation shell, and it is part of the first solvation shell of HCO_3^-. A hydrogen bond (HB) is formed between the hydroxide ion and HCO_3^-. (c) a proton transfer (PT) event occurs between the hydroxide ion and HCO_3^-, creating CO_3^{2-} and a water molecule (i.e., the forward path of reaction (2)). Yellow and green spheres represent previously hydroxide oxygen. (d) a HB is formed between CO_3^{2-} and a nearby water molecule. (e) a PT occurred between CO_3^{2-} and the water molecule, creating HCO_3^- and a hydroxide ion (i.e., the backward path of reaction (2)). Green sphere represents the newly formed hydroxide ion. (f) The hydroxide ion is back into the BR in a threefold stable structure. (g) A typical stable $OH^-(H2O)_5$ structure formed in the BR, similar to the structure shown in Figure a. (h) A typical water structure formed in the BR without the presence of a hydroxide ion. The red, white, turquoise, and blue spheres represent O, H, C, and N atoms, respectively. The yellow and green spheres represent the instantaneous hydroxide oxygens, HCO_3^- and CO_3^{2-}. The yellow and green arrows demonstrate the green and yellow hydroxide ion spheres diffusion path, respectively.

5. Discussion and Conclusions

In this combined theoretical and experimental study, we explored the carbonation process in AEMs and the effect of carbonate ions on the hydroxide ion solvation structure and diffusion. From fully atomistic AIMD simulations of idealized nano-confined AEMs that contains CO_2 in their initial structure, we found that the hydroxide ions were more likely to react with CO_2 in low-hydration conditions. This is due to the main reaction barrier for the reaction $OH^- + CO_2 \rightarrow HCO_3^-$ bringing the OH^- into the first solvation shell of CO_2, which is significantly reduced in low-hydration conditions. For moderate hydration values ($\lambda = 10$), we did not observe any reaction between the hydroxide ion and CO_2. Additionally, once the initial condition contained CO_3^{2-}, the backward path of reaction (2) was preferred in low-hydration conditions. For all systems, OH^- and HCO_3^- were the most common species to exist along the simulation. Hence, we conclude that exposing low-hydrated systems under confined environments to ambient air appears to result in the creation of HCO_3^-. However, keeping the system at moderate to high hydration values may postpone the reaction between the hydroxide ion and CO_2, thus extending AEM lifetime.

Exploring the solvation structures of the ions in the systems revealed that as a result of the larger size of HCO_3^- and the geometrical constrains of the TMA cations, the HCO_3^- are less hydrated than in a bulk solution. As there are less hydroxide ions in the system, the water molecules are divided between HCO_3^- and OH^-. Thus, the water uptake in the first and second solvation shells of the hydroxide ion increases in low-hydrated AEMs. As the hydroxides are more hydrated in the presence of carbonate ions, the shielding between the hydroxide ion and cationic group is higher, which, in turn, can decrease the degradation process, as was recently reported in Ref. [22].

While the increase in CN of the first and second solvation shells of the hydroxide ions suggest an improved ionic conductivity, we discovered, both theoretically and experimentally, that the hydroxide ion diffusivity is significantly reduced in the presence of carbonate ions. Additionally, water molecules and the three carbon-containing species exhibited a non-diffusive behavior. Exploration of the AIMD trajectories revealed that the non-diffusive carbonate ions are “blocking” the hydroxide ions from flowing along the simulation cell. In our previous work on low hydrated AEMs we discovered that the region between each pair of cations create a BR

for hydroxide diffusion, as only specific solvation structures are diffusive, leading to a suppression of hydroxide ion mobility. [40,42,43] In the current simulations, we identified that even in cases in which the hydroxide achieved the structures allowing them to cross the BR, the carbonate ions are "blocking them from diffusing into the CCR, and are driving them back into the BR. To overcome this obstacle, we suggest expanding the BR in future work, in order to reduce the "blocking area", as this should allow the hydroxide ions to diffuse along the BR and into the next CCR.

To the best of our knowledge, this work is the first to provide atomistic insights and a preliminary fundamental understanding on the carbonation process in AEMs and its effects on hydroxide ion solvation structure and diffusion. We believe our results enable us to suggest novel design strategies to improve hydroxide ion conductivity in high-performance AEMFCs in the presence of CO_2 containing air.

Supplementary Information

The following additional data are presented in the Supplementary Information (SI): (i) Computational methods, system parameters, and the choice of hydration values; (ii) OO, NO_w and NO^* RDFs and CNs; (iii) MSD explanation; (iv) diffusion coefficients along each of the axes separately; (v) O*O CN values for 1st and 2nd solvation shells; (vi) hydroxide ions and carbonate anions coordinates as a function of time; (vii) additional results to Figure 4, at different initial conditions; and (viii) experimental details.

Conflict of Interest

There are no conflicts to declare.

Acknowledgments

This work was supported by the National Science Foundation, grant # CHE-1534374 (T.Z., M.E.T.) and by the United States-Israel Binational Science Foundation (BSF), grant #2018171 (T.Z., D.R.D., and M.E.T.). Computational resources were provided by the Computational Center for Nanotechnology Innovation at Rensselaer Polytechnic Institute in Troy, New York. Partial support from the Nancy & Stephen Grand Technion Energy Program

(GTEP) and the Ministry of National Infrastructure, Energy and Water Resources of Israel through grant No. 3-17591 (22-11-040) is also acknowledged (D.R.D.). I.N. and C.S. acknowledge the MISE FISR 2019 AMPERE project (FISR2019_01294) for the financial support.

References

[1] G. Merle, M. Wessling, and K. Nijmeijer, "Anion Exchange Membranes for Alkaline Fuel Cells: A Review," *J. Memb. Sci.*, 377, 1–35, 2011.

[2] J. Pan, C. Chen, L. Zhuang, and J. Lu, "Designing Advanced Alkaline Polymer Electrolytes for Fuel Cell Applications," *Acc. Chem. Res.*, 45, 473–481, 2012.

[3] M. A. Hickner, A. M. Herring, and E. B. Coughlin, "Anion Exchange Membranes : Current Status and Moving Forward," *J. Polym. Sci. PART B Polym. Phys.*, 51, 1727–1735, 2013.

[4] D. R. Dekel, "Alkaline Membrane Fuel Cell (AMFC) Materials and System Improvement - State-of-the-Art," *ECS Trans.*, vol. 50, pp. 2051–2052, 2013.

[5] K. W. Han, K. H. Ko, K. Abu-hakmeh, C. Bae, Y. J. Sohn, and S. S. Jang, "Molecular Dynamics Simulation Study of a Polysulfone-Based Anion Exchange Membrane in Comparison with the Proton Exchange Membrane," *J. Phys. Chem. C*, 118, 12577−12587, 2014.

[6] C. Chen, Y.-L. S. Tse, G. E. Lindberg, C. Knight, and G. A. Voth, "Hydroxide Solvation and Transport in Anion Exchange Membranes," *J. Am. Chem. Soc.*, 138, 991–1000, 2016.

[7] D. R. Dekel, "Review of Cell Performance in Anion Exchange Membrane Fuel Cells," *J. Power Sources*, 375, 158–169, 2018.

[8] S. Gottesfeld, D. R. Dekel, M. Page, C. Bae, Y. Yan, P. Zelenay, and Y. S. Kim, "Anion Exchange Membrane Fuel Cells: Current Status and Remaining Challenges," *J. Power Sources*, 375, 170–184, 2018.

[9] K. F. L. Hagesteijn, S. Jiang, and B. P. Ladewig, "A Review of the Synthesis and Characterization of Anion Exchange Membranes," *J. Mater Sci*, 53, 11131–11150, 2018.

[10] W. You, K.J.T. Noonan, G. W.Coates, "Alkaline-Stable Anion Exchange Membranes: A Review of Synthetic Approaches", *Prog. Polym. Sci.* 100, 101177–101189, 2020.

[11] C. Li, and J.-B. Baek, "The Promise of hydrogen Production From Alkaline Anion Exchange Membrane Electrolyzers", *Nano Energy.* 87, 106162–106179, 2021.

[12] J. Biemolt. J. C. Douglin, R. K. Singh, E. S Davydova, N. Yan, G. Rothenberg and D. R. Dekel, "An Anion-Exchange Membrane fFel Cell Containing Only Abundant and Affordable Materials," *Energy Technol.*, 9, 2000909–2000913, 2021.

[13] D. R. Dekel, S. Willdorf, U. Ash, M. Amar, S. Pusara, S. Dhara, S. Srebnik, and C. E. Diesendruck, "The Critical Relation Between Chemical Stability of Cations and Water in Anion Exchange Membrane Fuel Cells Environment," *J. Power Sources*, 375, 351–360, 2018.

[14] C. E.Diesendruck and D. R.Dekel, "Water – A Key Parameter in the Stability of Anion Exchange Membrane Fuel Cells," *Curr. Opin. Electrochem.*, 9, 173–178, 2018.

[15] J. Xue, J. Zhang, X. Liu, T. Huang, H. Jiang, Y. Yin, Y. Qin, and M. D. Guiver, "Toward Alkaline-Stable Anion Exchange Membranes in Fuel Cells: Cycloaliphatic Quaternary Ammonium-Based Anion Conductors," *Electrochem. Energy Rev.*, 2021.

[16] J. Peng, A. L. Roy, S. G. Greenbaum, and T. A. Zawodzinskia, "Effect of CO_2 Absorption on Ion and Water Mobility in an Anion Exchange Membrane," *J. Power Sources*, 380, 64–75, 2018.

[17] Z. Siroma, S. Watanabe, K. Yasuda, K. Fukuta, and H. Yanagi, "Mathematical Modeling of the Concentration Profile of Carbonate Ions in an Anion Exchange Membrane Fuel Cell," *J. Electrochem. Soc*, 158, B682−B689, 2011.

[18] G. Li, Y. Wang, J. Pan, J. Han, Q. Liu, X. Li, P. Li, C. Chen, L. Xiao, J. Lu, and L. Zhuang, "Carbonation Effects on the Performance of Alkaline Polymer Electrolyte Fuel Cells," *Int. J. Hydrogen Energy*, 40, 6655–6660, 2015.

[19] N. Ziv and D. R. Dekel, "A Practical Method for Measuring the True Hydroxide Conductivity of Anion Exchange Membranes," *Electrochem. commun.*, 88, 109–113, 2018.

[20] N. Ziv, W. E. Mustain, and D. R. Dekel, "The Effect of Ambient Carbon Dioxide on Anion-Exchange Membrane Fuel Cells," *ChemSusChem*, 11, 1136–1150, 2018.

[21] U. Krewer, C. Weinzierl, N. Ziv, and D. R. Dekel, "Impact of carbonation processes in anion exchange membrane fuel cells," *Electrochim. Acta*, 263, 433–446, 2018.

[22] S. Srebnik, S. Pusara, and D. R. Dekel, "Effect of Carbonate Anions on Quaternary Ammonium-Hydroxide Interaction," *J. Phys. Chem. C*, 123, 15956−15962, 2019.

[23] Y. Zheng, L. N. I. Colon, N. U. Hassan, E. R. Williams, M. Stefik, J. M. LaManna, D. S. Hussey, and W. E. Mustain, "Effect of Membrane Properties on the Carbonation of Anion Exchange Membrane Fuel Cells," *Membranes (Basel).*, 11, 102–115, 2021.

[24] I. Zadok, D. R. Dekel, and S. Srebnik, "Effect of Ammonium Cations on the Diffusivity and Structure of Hydroxide Ions in Low Hydration Media," *J. Phys. Chem. C*, 123, 27355–27362, 2019.

[25] I. Zadok, H. Long, B. Pivovar, A. Roznowska, A. Michalak, D. R. Dekel, and S. Srebnik, "Unexpected Hydroxide Ion Structure and Properties at Low Hydration," *J. Mol. Liq.*, 313, 113485–113495, 2020.

[26] M. E. Tuckerman, "*Ab Initio* Molecular Dynamics: Basic Concepts, Current Trends and Novel Applications," *J. Phys. Condens. Matter*, 14, R1297–R1355, 2002.

[27] D. Marx and J. Hutter, *Ab Initio Molecular Dynamics: Theory and Implementation, in Modern Methods and Algorithms of Quantum Chemistry*, Vol.1. Juelich: Forschungszentrum, 2000.

[28] B. F. Habenicht, S. J. Paddison, and M. E. Tuckerman, "Ab *Initio* Molecular Dynamics Simulations Investigating Proton Transfer in Perfluorosulfonic Acid Functionalized Carbon Nanotubes," *Phys. Chem. Chem. Phys.*, 12, 8728–8732, 2010.

[29] B. F. Habenicht, S. J. Paddison, and M. E. Tuckerman, "The Effects of the Hydrophobic

Environment on Proton Mobility in Perfluorosulfonic Acid Systems: An Ab *Initio* Molecular Dynamics Study," *J. Mater. Chem.*, 20, 6342–6351, 2010.

[30] M. A. Modestino, D. K. Paul, S. Dishari, S. A. Petrina, F. I. Allen, M. A. Hickner, K. Karan, R. A. Segalman, and A. Z. Weber, "Self-Assembly and Transport Limitations in Confined Nafion Films," *Macromolecules*, 46, 867−873, 2013.

[31] A. Kusoglu, D. Kushner, D. K. Paul, K. Karan, M. A. Hickner, and A. Z. Weber, "Impact of Substrate and Processing on Confinement of Nafion Thin Films," *Adv. Funct. Mater*, 24, 4763–4774, 2014.

[32] K. A. Page, A. Kusoglu, C. M. Stafford, S. Kim, R. J. Kline, and A. Z. Weber, "Confinement-Driven Increase in Ionomer Thin-Film Modulus," *Nano Lett.*, 14, 2299−2304, 2014.

[33] J. K. Clark II, B. F. Habenicht, and S. J. Paddison, "Ab *Initio* Molecular Dynamics Simulations of Aqueous Triflic Acid Confined in Carbon Nanotubes," *Phys. Chem. Chem. Phys.*, 16, 16465–16479, 2014.

[34] D. Muñoz-Santiburcio, D. Marx, "On the Complex Structural Diffusion of Proton Holes in Nanoconfined Alkaline Solutions Within Slit Pores", *Nat. Commun.* 7, 12625–12633, 2016

[35] A. Kusoglu and A. Z. Weber, "New Insights into Perfluorinated Sulfonic-Acid Ionomers," *Chem. Rev.*,117, 987−1104, 2017.

[36] J. G. Brandenburg, A. Zen, D. Alfè, and A. Michaelides, "Interaction Between Water and Carbon Nanostructures: How Good Are Current Density Functional Approximations?," *J. Chem. Phys*, 151, 164702–164713, 2019.

[37] S. Faucher, N. Aluru, M.Z. Bazant, D. Blankschtein, A.H. Brozena, J. Cumings, J.P. de Souza, M. Elimelech, R. Epsztein, J.T. Fourkas, A.G. Rajan, H.J. Kulik, A. Levy, A. Majumdar, C. Martin, M. McEldrew, R.M. Prasanna, A. Noy, T.A. Pham, M. Reed, E. Schwegler, Z. Siwy, Y. Wang, M. Strano, "Critical Knowledge Gaps in Mass Transport through Single-Digit Nanopores: A Review and Perspective", *J. Phys. Chem. C.* 123, 21309−21326, 2019.

[38] D. Muñoz-Santiburcio, D. Marx, "Confinement-Controlled Aqueous Chemistry within Nanometric Slit Pores", *Chem. Rev.* 121, 6293−6320, 2021.

[39] T. Zelovich, Z. Long, M. Hickner, S. J. Paddison, C. Bae, and M. E. Tuckerman, "Ab initio Molecular Dynamics Study of Hydroxide Diffusion Mechanisms in Nano-Confined Structural mimics of Anion Exchange Membranes," *J. Phys. Chem. C*, 123, 4638–4653, 2019.

[40] T. Zelovich, L. Vogt-Maranto, M. A. Hickner, S. J. Paddison, C. Bae, D. R. Dekel, and M. E. Tuckerman, "Hydroxide Ion Diffusion in Anion Exchange Membranes at Low Hydration: Insights from Ab *initio* Molecular Dynamics," *Chem. Mater*, 31, 5778–5787, 2019.

[41] T. Zelovich and M. E. Tuckerman, "Water Layering Affects Hydroxide Diffusion in Functionalized Nanoconfined Environments," *J. Phys. Chem. Lett*, 11, 5087–5091, 2020.

[42] T. Zelovich, K. I. Winey, and M. E. Tuckerman, "Hydronium Ion Diffusion in Model Proton Exchange Membranes at Low Hydration: Insights from Ab Initio Molecular Dynamics," *J. Mat. Chem. A*, 9, 2448–2458, 2021.

[43] T. Zelovich and M. E. Tuckerman, "OH^- and H_3O^+ Diffusion in Model AEMs and PEMs at Low Hydration: Insights from Ab *Initio* Molecular Dynamics," *Membranes*, 11, 355–368, 2021.

[44] T. Zelovich, L. Vogt-Maranto, C. Simari, I. Nicotera, M. Hickner, S. J. Paddison, C. Bae, D. R. Dekel and M. E. Tuckerman, "Non-Monotonic Temperature Dependence of Hydroxide Diffusion in Anion Exchange Membranes," *Chem. Mater.* 23, 2133−2145, 2022.

[45] T. Zelovich and M. E. Tuckerman, "Controlling Hydronium Diffusivity in Model Proton Exchange Membranes," *J. Phys. Chem. Lett.* 13, 2245-2253, 2022.

[46] M. E. Tuckerman, K. Laasonen, M. Sprik, and M. Parrinello, "*Ab Initio* Molecular Dynamics Simulation of the Solvation and Transport of Hydronium and Hydroxide Ions in Water," *J. Chem. Phys.*, 103, 150-161, 1995.

[47] M. Tuckerman, K. Laasonen, M. Sprik, and M. Parrinello, "Ab Initio Molecular

Dynamics Simulation of the Solvation and Transport of H3O+ and OH- Ions in Water," *J. Phys. Chem*, 99, 5749–5752, 1995.

[48] D. Marx, M. E. Tuckerman, J. Hutter, and M. Parrinello, "The Nature of the Hydrated Excess Proton in Water," *Nature*, 397, 601–604, 1999.

[49] M. E. Tuckerman, D. Marx, and M. Parrinello, "The Nature and Transport Mechanism of Hydrated Hydroxide Ions in Aqueous Solution," *Nature*, 417, 925–929, 2002.

[50] Z. Zhu and M. E. Tuckerman, "Ab Initio Molecular Dynamics Investigation of the Concentration Dependence of Charged Defect Transport in Basic Solutions via Calculation of the Infrared Spectrum," *J. Phys. Chem. B*, 106, 8009–8018, 2002.

[51] M. E. Tuckerman, A. Chandra, and D. Marx, "Structure and Dynamics of OH - (aq)," *Acc. Chem. Res.*, 39, 151–158, 2006.

[52] A. Chandra, M. E. Tuckerman, and D. Marx, "Connecting Solvation Shell Structure to Proton Transport Kinetics in Hydrogen – Bonded Networks via Population Correlation Functions," *Phys. Rev. Lett*, 99, 145901–145904, 2007.

[53] D. Marx, A. Chandra, and M. E. Tuckerman, "Aqueous Basic Solutions : Hydroxide Solvation , Structural Diffusion , and Comparison to the Hydrated Proton," *Chem. Rev.*, 110, 2174–2216, 2010.

[54] M. E. Tuckerman, A. Chandra, and D. Marx, "A Statistical Mechanical Theory of Proton Transport Kinetics in Hydrogen-Bonded Networks Based On Population Correlation Functions With Applications to Acids and Bases," *J. Chem. Phys.*, 133, 124108–124129, 2010.

[55] Z. Ma and M. E. Tuckerman, "On the Connection Between Proton Transport , Structural Diffusion , and Reorientation of the Hydrated Hydroxide Ion as a Function of Temperature," *Chem. Phys. Lett*, 511, 177–182, 2011.

[56] A. Hassanali, M. K. Prakash, H. Eshet, and M. Parrinello, "On the Recombination of Hydronium and Hydroxide Ions in Water," *Proc. Natl. Acad. Sci. U.S.A.*, 108, 20401–20415, 2011.

[57] A. Bankura and A. Chandra, "Hydration Structure and Dynamics of a Hydroxide Ion in Water Clusters of Varying Size and Temperature: Quantum Chemical and Ab Initio Molecular Dynamics Studies," *Chem. Phys.*, 400,154–164, 2012.

[58] A. Hassanali, F. Giberti, J. Cuny, T. D. Kühne, and M. Parrinello, "Proton transfer through the water gossamer," *PNAS*,110, 13723–13728, 2013.

[59] N. Agmon, H. J. Bakker, R. K. Campen, R. H. Henchman, P.Pohl, S. Roke, M. Thamer, and A. Hassanali, "Protons and Hydroxide Ions in Aqueous Systems," *Chem. Rev.*, 116, 7642−7672, 2016.

[60] Y. Crespo and A. Hassanali, "Characterizing the Local Solvation Environment of OH− in Water Clusters with AIMD," *J. Chem. Phys.*, 144, 074304–074314, 2016.

[61] M. Chen, L. Zheng, B. Santra, H.-Y. Ko, R.A.D. Jr, M.L. Klein, R. Car, X. Wu, "Hydroxide Diffuses Slower Than Hydronium in Water Because its Solvated Structure Inhibits Correlated Proton Transfer", *Nat. Chem.* 10, 413–419, 2018

[62] P. Stilbs, "Fourier Transform Pulsed-Gradient Spin-Echo Studies of Molecular Diffusion," *Prog. NMR Spectrosc*, 19, 1–45, 1987.

[63] J. Karger, H. Pfeiffer, and W. Heink, "Principles and Application of Self Diffusion Measurements by Nuclear Magnetic Resonance," *Adv. Magn. Reson.*, 12, 1–89, 1988.

[64] W. S. Price, "Pulsed Field Gradient Nuclear Magnetic Resonance as a Tool for Studying Translational Diffusion: Part 1. Basic Theory," *Concepts Magn. Reson*, 9, 299–336, 1997.

[65] F. Sepehr, H. Liu, X. Luo, C. Bae, M. E. Tuckerman, M. A. Hickner, and S. J. Paddison, "Mesoscale Simulations of Anion Exchange Membranes Based on Quaternary Ammonium Tethered Triblock Copolymers," *Macromolecules*, 50, 4397–4405, 2017.

[66] D. R. Dekel, M. Amar, S. Willdorf, M. Kosa, S. Dhara, and C. E. Diesendruck, "Effect of Water on the Stability of Quaternary Ammonium Groups for Anion Exchange Membrane Fuel Cell Applications," *Chem. Mater*, 29, 4425−4431, 2017.

[67] M. G. Marino and K. D. Kreuer, "Alkaline Stability of Quaternary Ammonium Cations

for Alkaline Fuel Cell Membranes and Ionic Liquids," *ChemSusChem*, 8, 513–523, 2015.

[68] S. Chempath, J. M. Boncella, L. R. Pratt, N. Henson, and B. S. Pivovar, "Density Functional Theory Study of Degradation of Tetraalkylammonium Hydroxides," *J. Phys. Chem. C*,114, 11977–11983, 2010.

[69] S. Castaneda and R. Ribadeneira, "Theoretical Description of the Structural Characteristics of the Quaternized SEBS Anion-Exchange Membrane Using DFT," *J. Phys. Chem. C*, 119, 28235−28246, 2015.

[70] G. Yang, J. Hao, J. Cheng, N. Zhang, G. He, F. Zhang, and C. Hao, "Hydroxide Ion Transfer in Anion Exchange Membrane : A Density Functional Theory Study," *Int. J. Hydrogen Energy*, 41, 6877–6884, 2016.

[71] D. M. J. Hutter, A. Alavi, T. Deutsch, M. Bernasconi, S. Goedecker and M. T. and M. Parrinello, "CPMD, IBM Corporation 1990–2009 and MPI für Festkörperforschung 1997–2001; see www.cpmd.org, 2009." .

[72] G. J. Martyna and M. L. Klein, "Nose-Hoover Chains: The Canonical Ensemble via Continuous Dynamics," *J. Chem. Phys.*, 97, 2635–2643, 1992.

[73] A. D. Becke, "Density-Functional Exchange-Energy Approximation With Correct Asymptotic Behavior," *Phys. Rev. A*, 38, 3098–3100, 1988.

[74] C. Lee, W. Yang, and R. G. Parr, "Development of the Colle-Salvetti Correlation-Energy Formula into A Functional of the Electron Density," *Phys. Rev. B*, 37, 785–789, 1988.

[75] G. R. Jenness, O. Karalti, and K. D. Jordan, "Benchmark Calculations of Water–Acene Interaction Energies: Extrapolation to The Water–Graphene Limit and Assessment of Dispersion–Corrected DFT Methods," *Phys. Chem. Chem. Phys.*, 12, 6375–6381, 2010.

[76] I.-C. Lin, A. P. Seitsonen, I. Tavernelli, and U. Rothlisberger, "Structure and Dynamics of Liquid Water from ab Initio Molecular Dynamics - Comparison of BLYP, PBE, and revPBE Density Functionals with and without van der Waals Corrections," *J. Chem. Theory Comput*, 8,3902−3910, 2012.

[77] C. Simari, E. Lurfrano, M. H. U. Rehman, A. Zhegur-Khais, S. Haj-Bsoul, D. R. Dekel,

and I. Nocitera, "Effect of LDH Platelets on the Transport Properties and Carbonation of Anion Exchange Membrane," *Electrochim. Acta,* 403*,* 139713-139723, 2021.

[78] P. Ryszard and M. Wladyslaw, "Kintetics of Reaction Between Carbon Dioxide and Hydroxyl Ions in Aqueous Electrolyte Solutions," *Chem. Eng. Sci.*, 43, 1677–1684, 1988.

[79] M. Falk and A. G. Miller, "Infrared Spectrum of Carbon Dioxide in Aqueous Solution," *Vib. Spectrosc*, 4, 105–108, 1992.

[80] M. In Het Panhuis, C. H. Patterson, and R. M. Lynden-Bell, "A Molecular Dynamics Study of Carbon Dioxide in Water: Diffusion, Sructure and Thermodynamics," *Mol. Phys.*, 94, 963–972, 1998.

[81] K. Leung, I. M. B. Nielsen, and I. Kurtz, "Ab Initio Molecular Dynamics Study of Carbon Dioxide and Bicarbonate Hydration and the Nucleophilic Attack of Hydroxide on CO2," *J. Phys. Chem. B*, 111, 4453–4459, 2007.

[82] A. Stirling, "HCO_3^- Formation from CO_2 at High pH: Ab Initio Molecular Dynamics Study," *J. Phys. Chem. B*, 115, 14683–14687, 2011.

[83] A. Tongraar, P. Yotmanee, and A. Payaka, "Characteristics of CO32- Water Hydrogen Bonds in Aqueous Solution: Insights From HF/MM and B3LYP/MM MD Simulations," *Phys. Chem. Chem. Phys*,13, 16851–16860, 2011.

[84] X. Shi, H. Xiao, K. S. Lackner, and X. Chen, "Capture CO_2 from Ambient Air Using Nanoconfined Ion Hydration," *Angew. Chem. Int. Ed*, 55, 4026 –4029, 2016.

[85] X. Shi, H. Xiao, X. Chen, and K. S. Lackner, "The Effect of Moisture on the Hydrolysis of Basic Salts," *Chem. Eur. J.*, 22, 18326 – 18330, 2016.

[86] H. Xiao, X. Shi, Y. Zhang, X. Liao, F. Hao, K. S. Lackner, and X. Chen, "The Catalytic Effect of H_2O on the Hydrolysis of CO_3^{2-} in Hydrated Clusters and its Implication in the Humidity Driven CO_2 Air Capture," *Phys.Chem.Chem.Phys*, 19, 27435-27441, 2017.

[87] N. Ziv, W. E. Mustain, and D. R. Dekel, "The Effect of Ambient Carbon Dioxide on Anion-Exchange Membrane Fuel Cells," *ChemSusChem*, 11, 1136–1150, 2018.